vibration

MDPI

Article

A Vibrometer Based on Magnetorheological Optical Resonators

Edoardo Rubino [1,*] and Tindaro Ioppolo [2]

[1] Mechanical and Industrial Engineering Department, University of Wisconsin Platteville, Platteville, WI 53818, USA
[2] Mechanical Engineering Department, Southern Methodist University, Dallas, TX 75275, USA; ioppolo@lyle.smu.edu
* Correspondence: rubinoe@uwplatt.edu; Tel.: +1-(608)-342-6058

Received: 23 August 2018; Accepted: 9 October 2018; Published: 17 October 2018

Abstract: This paper addresses the feasibility of an optical vibrometer that is based on the shift of the optical modes, also known as whispering gallery modes (WGMs), of a magnetorheological optical resonator. The optical resonator that is used in this study is fabricated by mixing polyvinyl chloride plastisol with magnetically polarizable particles. When a permanent magnet that is located nearby the optical resonator is moved, it induces a perturbation of the morphology of the resonator, due to the magnetostrictive effect. This change in the morphology induces a shift in the optical modes of the resonator. The shift of the optical modes can be related to the displacement of the permanent magnet. The proposed sensor concept is based on monitoring the displacement of a tiny magnet that is attached to a moving surface. The optical quality factor of the resonator used in these studies was of the order of 10^6. The experimental results show a sensitivity of 0.32 pm/μm and a resolution that is less than 300 nm.

Keywords: vibrometer; magnetorheological; optical resonator; composites; smart materials; whispering gallery modes

1. Introduction

Several techniques have been developed so far, to detect and monitor the amplitude and the frequency of the displacement of vibrating systems. Laser vibrometers are interferometric instruments [1] that make use of the coherence properties of a laser beam [2]. A laser light is pointed toward the vibrating object, and the backscattered light is detected with a photodiode. By comparing the Doppler frequency between the source beam and the backscattered light [3], it is possible to determine the vibrating characteristics of the tested object. Laser vibrometers have been studied extensively [4], and they are employed in several fields such as structural health monitoring [5,6] and fruit textural changes [7,8]. Other studies reported that it is possible to obtain a resolution of the order of attometers with this technique [9]. Other optical methods have been developed to determine the displacement of vibrating objects. Light emission diodes (LED) were, for instance, used to measure the bending and torsional vibrations of pipes [10–12]: the pipe is located between a projector and a receiver to create a shaded area on the receiver. The vibration of the pipe can then be detected by measuring the amount of light that reaches the receiver. With this technique, a resolution of 60 nm can be obtained, and the sensor size is in the order of tens of centimeters. Optical digital techniques have been developed to detect the displacement of flexible bridges for structural analysis purposes [13]: the motion of a marked panel placed on the bridge was followed by a camera placed on a fixed point, and the recorded images were analyzed through digital image processing software. The resolution and

sensitivity of the proposed device are a function of the camera and lenses used, as well as the distance between the camera and the targeted point.

Another optical system that is used to develop vibrometers makes use of an optical fiber that points the light to the surface of the vibrating object and of a photodiode that measures the variation of the intensity of the reflected light [14,15]. With this method, a sensitivity of 0.893 V/mm in the frequency range between 75 and 275 Hz was obtained. Also, this technique was used for multipoint measurements [16], obtaining a resolution in the order of 1 µm. Another study reported the optical detection of the resonant frequency of a quartz crystal resonator [17]. A resolution in the order of 10 µm has been reached in developing a displacement sensor based on a Fabry-Perot device [18], or of 142 µm with a vibrometer for cryogenic applications based on fiber Bragg gratings [19]. In addition, recent studies have reported that the optical-knife edge technique allows for displacement measurements in the range between 13 MHz and 895 MHz, with a resolution of 455 fm/$\sqrt{}$Hz [20]. In this paper, we present a novel technique to measure the out-of-plane displacement of a vibrating object or surface. The sensing concept is based on the shift of the morphology-dependent resonances (MDR), also known as whispering gallery modes (WGM) of a magnetorheological spherical resonator. The WGM phenomenon has been used in the past for various applications, due to the high optical quality factor of the optical modes. These micro-cavities have been used for the development of devices for telecommunication (filtering, switches, multiplexing, etc.) [21–24] as well as mechanical [25–32], thermal [33–36], and biological [37–42] sensing applications.

2. Sensor Concept

The proposed sensing modality exploits the optical modes of spherical dielectric optical resonators. The optical resonances in a spherical resonator can be described using geometric optics as long as the wavelength of the light that is used to excite the optical modes is much smaller than the radius of the resonator. Using this description, an optical resonance is excited when the length of the path of the light traveling on the internal surface of the resonator is a multiple integer of the wavelength, namely when $2\pi rn = l\lambda$, where r is the radius of the microsphere, l is an integer, n is the index of refraction of the resonator and λ is the wavelength of the light. Figure 1 shows the coupling of the optical fiber and the optical resonator.

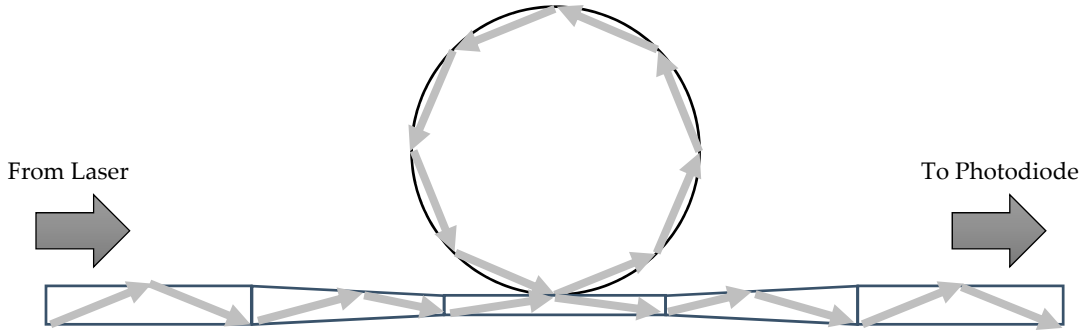

Figure 1. Schematic of the path of the light from the fiber to the resonator and back to the fiber.

When excited, the optical resonances, also known as optical modes or Whispering Gallery Modes (WGMs), are seen as sharp dips in the transmission spectrum (see Figure 2). If the radius or the index of refraction (or both) of the resonator are perturbed by an external effect, a shift of the optical modes ($\Delta\lambda$) can be written as follows:

$$\frac{\Delta\lambda}{\lambda} = \frac{\Delta r}{r} + \frac{\Delta n}{n} \quad (1)$$

The variation of the radius and the index of refraction of the microsphere represent the strain effect and stress effect respectively. However, as reported in previous studies [43,44] the stress effect

is negligible compared with the strain effect. Therefore, the relative shift of the optical modes can be expressed as $\Delta\lambda/\lambda = \Delta r/r$.

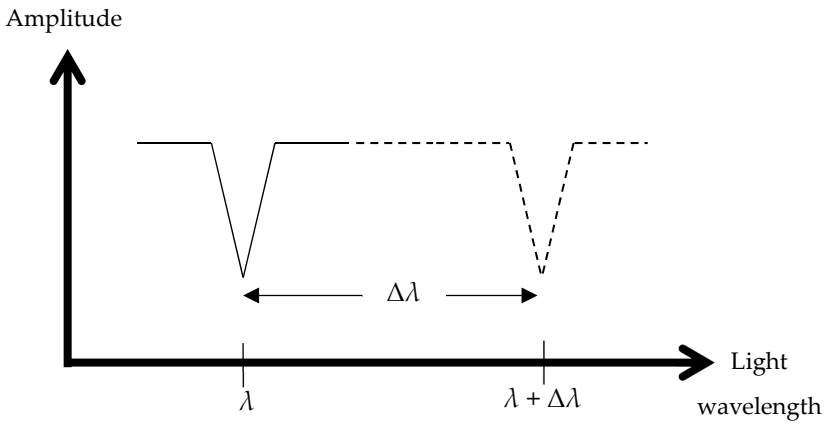

Figure 2. Schematic of the transmission spectrum.

To demonstrate the proposed sensing modality, we used a polymeric optical resonator that is doped with magnetically polarizable particles. When the resonator is placed in the vicinity of a permanent magnet, the magnetic forces acting on it will induce an elastic deformation and therefore a shift of the optical modes. When the permanent magnet is attached to a vibrating object, the amplitude of the vibration can be measured by placing the optical resonator in the proximity of the vibrating magnet and by observing the shift of the optical modes in the transmission spectrum (see Figure 2).

3. Analysis

Here, we assumed that the magnetorheological micro-optical resonator is placed nearby the surface of a movable tiny permanent magnet, as shown in Figure 3.

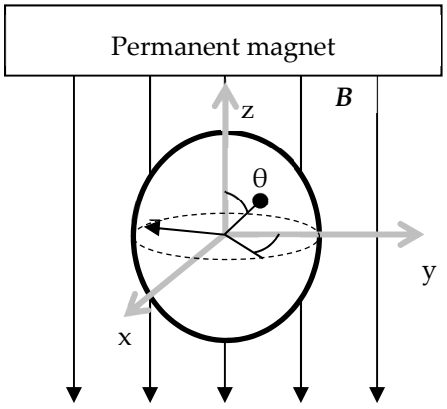

Figure 3. Schematic of the microsphere subjected to the inductive magnetic field B generated by the permanent magnet. θ, x, y and z are the spatial coordinates.

Since the magnet is allowed to move in the direction parallel to the z-axis (see Figure 3), the intensity of the inductive magnetic field at the microsphere location changes, inducing changes in the magnetic force acting on it. These forces, acting on the optical resonator, induce a shift in the optical resonances as in [43]:

$$\frac{\Delta\lambda}{\lambda} = -\frac{7-4\nu}{4G(7+5\nu)}\left[(\mu_r-1)^2+\frac{b_1-b_2}{\mu_0}\right]\frac{3B^2}{\mu_0(\mu_r+2)^2} \quad (2)$$

where G, ν, and μ_r are respectively, the shear modulus, the Poisson ratio, and the relative magnetic permeability of the microsphere. Coefficients b_1 and b_2 are defined as $b_1 = \partial\mu\partial e_{ii}$ and $b_2 = \partial\mu\partial e_{kk}$, where e_{ii} and e_{kk} are the normal components of the strain. The magnetic permeability of the surrounding fluid (air) is close to that of the vacuum, and it is indicated with μ_0. B is the intensity of the external inductive magnetic field.

The above relationship shows that the WGM shift is a quadratic function of the applied external inductive magnetic field, and it is also a function of the elastic and magnetic properties of the optical resonator. If the spatial distribution of the inductive magnetic field is known, the induced WGM shift can be related to the position of the magnet. Thus, Equation (2) can be written as:

$$\frac{\Delta\lambda}{\lambda} = k\, B(z)^2 \tag{3}$$

where $k = -\left\{\frac{[3(7-4\nu)]}{[4G(7+5\nu)\mu_0(\mu_r+2)^2]}\right\}\left\{(\mu_r-1)^2 + \frac{b_1-b_2}{\mu_0}\right\}$ (see Equation (2)). If we assume that the displacement of the magnet is relatively small, we can linearize Equation (3) as:

$$\frac{\Delta\lambda}{\lambda} = 2\, k\, B(Z_0)B'(Z_0)\Delta z \tag{4}$$

Here, Z_0 is the initial distance between the surface of the magnet and the center of the sphere, B' is its derivative and Δz is the displacement of the magnet. From the above equation, we can calculate the displacement as a function of the WGM shift. Therefore, if a magnet is placed on a moving surface, the displacement of that surface can be measured using the presented approach.

4. Results

A schematic of the optoelectronic setup used in this experiment is reported in Figure 4.

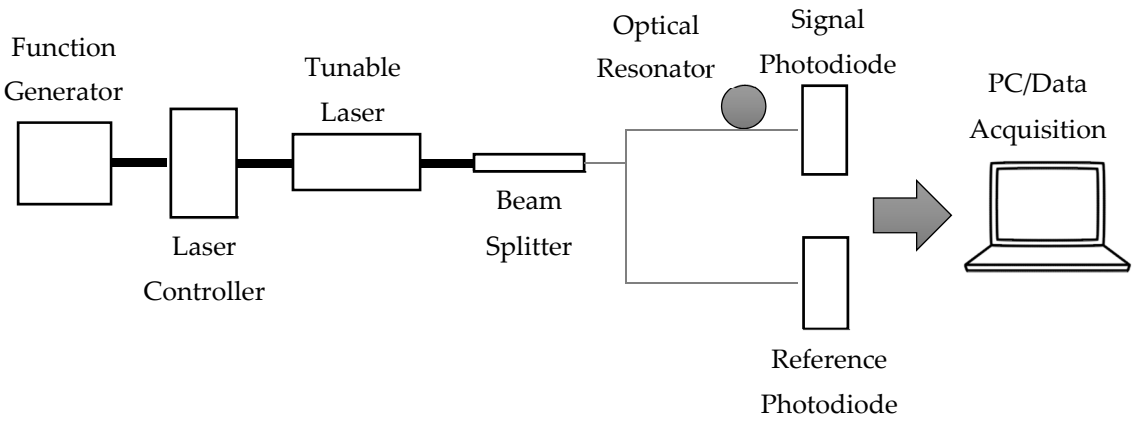

Figure 4. Schematic of the optoelectronic setup.

This is analogous to that one used in our previous studies [25,45]. Briefly, a single mode optical fiber is coupled to a tunable distributed feedback (DFB) laser diode that has a nominal central wavelength of 1.312 μm and 10 mW maximum power. A section of the optical fiber is tapered (by heating and stretching the fiber) to couple evanescently the laser light from the tapered fiber into the microsphere. The other end of the optical fiber is brought to a photodiode to monitor the transmission spectrum. The output from the photodiodes is analyzed with in-house software that calculates the WGM shift. The microsphere was fabricated using polyvinyl chloride-plastisol (PVC) that was mixed with magnetically polarizable particles. The mixture of polymer–magnetic particles was placed in an oven at a temperature of 230 °C for 20 min. The tip of an optical fiber with a diameter of 125 μm was immersed in the polymer mixture, and due to surface tension and gravity,

a spherical droplet was formed at the tip of the fiber. The solid sphere was formed by cooling it at room temperature. Once the solid sphere was formed, it was coated with a thin layer of pure polymer (PVC) that served as an optical wave-guide for the propagation of the optical modes. A photograph of a resonator used in this study is reported in Figure 5. It has a radius of ~600 μm and a volume fraction (the ratio between the volume of particles and the volume of the composite elastomer) of 0.32.

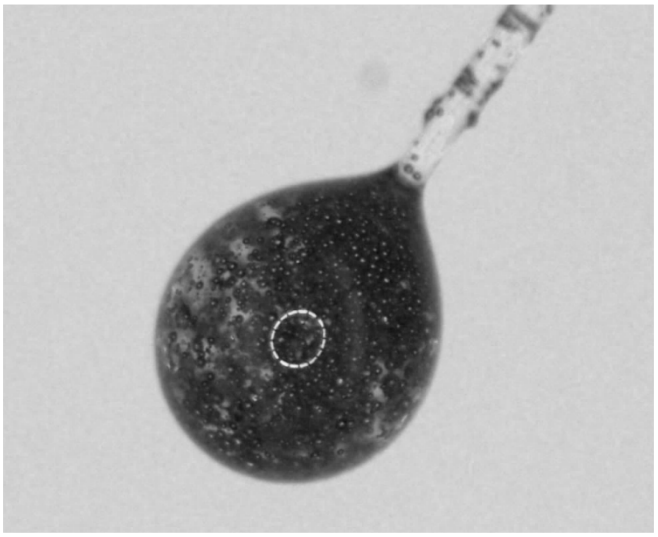

Figure 5. A picture of the magnetorheological spherical resonator.

An experiment was carried out to characterize the response of the elastic magnetorheological sphere to the applied external magnetic field. The microsphere was placed in a uniform inductive magnetic field that was generated by a magnetic coil. The intensity of the field was changed by changing the current flowing into the coil, and it was measured using a Gauss meter. In addition, the temperature was kept constant during the measurements. Figure 6 shows the relationship between the applied external inductive magnetic field and the induced WGM shift. As shown in the figure, there is a quadratic dependency between the induced WGM shift and the applied inductive magnetic field. In addition, we carried out a series of experiments where the optical resonator was placed near a disk-shaped permanent magnet (K&J Magnetics D8H2-Plumsteadville, PA, USA), axially magnetized with a thickness of 5.08 mm and a diameter of 12.7 mm, as shown in Figure 7.

Initially, the permanent magnet was placed on a translation stage, while the microsphere was kept steady at a distance Z_0 of 2 mm from the surface of the permanent magnet (see Figure 7).

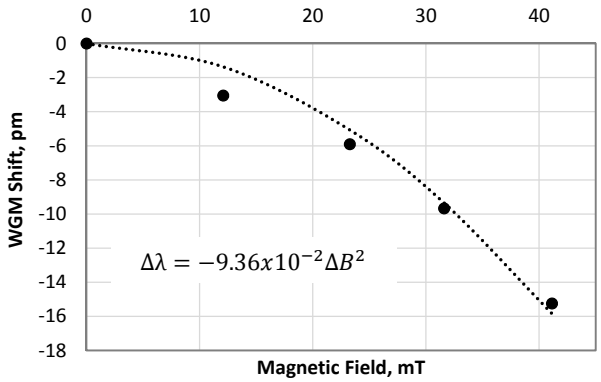

Figure 6. Relationship between the applied external inductive magnetic field and the whispering gallery mode (WGM) shift.

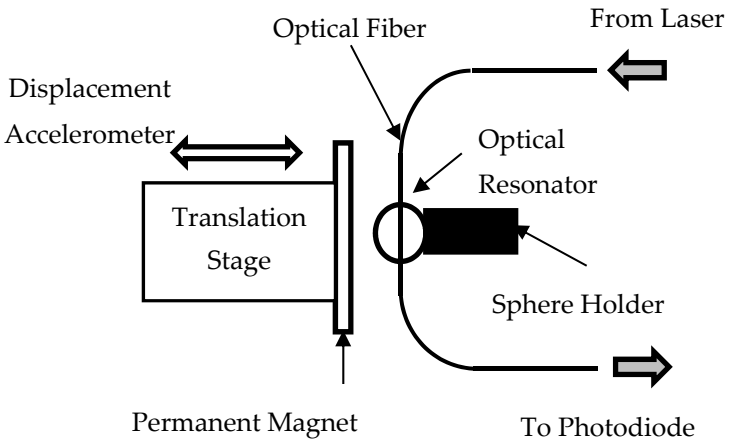

Figure 7. Schematic of the experimental setup.

The magnet was then moved in steps with an amplitude of 25.4 μm, and the WGM shift was recorded. Figure 8 shows the response of the optical resonator to the stepwise displacement of the permanent magnet. As shown in Figure 8, the WGM shift followed the position of the permanent magnet relative to the microsphere very well.

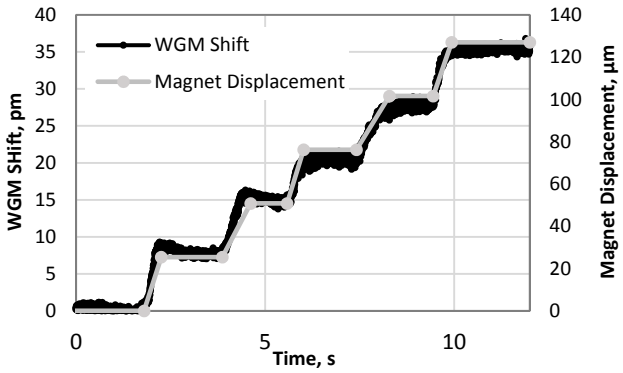

Figure 8. WGM shift and displacement of the permanent magnet as a function of time.

As the magnet is moved far away from the optical resonator, the WGM experienced a red shift, since the intensity of the inductive magnetic field decreased and the microsphere tended to reach its original size ($\Delta R > 0$).

Figure 9 shows the relationship between the displacement of the permanent magnet and the induced WGM shift together with the analytical results obtained from Equation (4) using the values of $B(Z_0)$ and $B'(Z_0)$ and k, discussed previously.

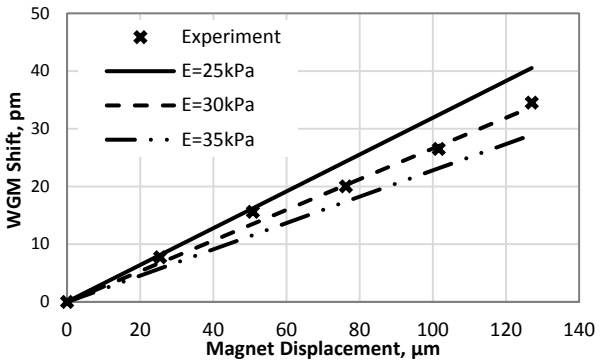

Figure 9. Relationship between the WGM shift and the displacement of the magnet.

As shown, there was a nearly linear relationship between the displacement of the magnet and the WGM shift. In the same figure, the values of the WGM shift (calculated using Equation (2)) for three different values of Young's modulus of the polymer (Young's modulus of the polymeric matrix varies ranges from 25 kPa to 35 kPa [28]) were also reported.

Measurements of the sensitivity were repeated for different values of the initial distance, Z_0, between the resonator and the surface of the permanent magnet. Figure 10 shows the results of these measurements. As expected, the sensitivity decreases with an increase of the distance between the permanent magnet and the optical resonator, since the strength of the inductive magnetic field decays with increasing distance.

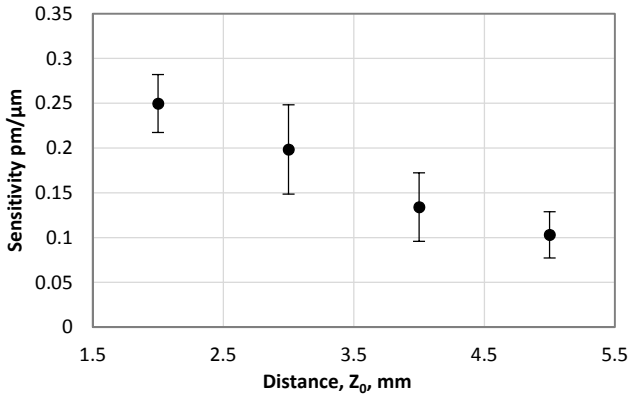

Figure 10. Sensitivity as a function of the initial distance between the permanent magnet and the optical resonator.

In addition to these studies, we carried out experiments to study the dynamic response of the optical resonator. For these experiments, the permanent magnet was mounted onto a plate connected to a shaker that was driven harmonically by a function generator. An accelerometer mounted on the movable plate was used to calculate the amplitude of the displacement of the permanent magnet. Figure 11 shows the WGM shift and the magnet displacement as a function of time for an input frequency of 30 Hz. As shown in figure, the WGM shift follows the displacement of the permanent magnet very well.

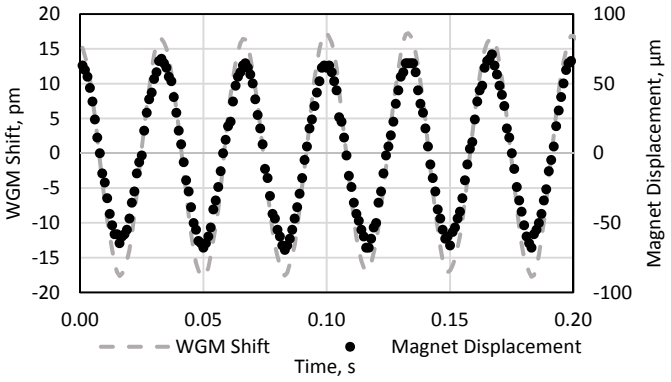

Figure 11. WGM shift induced by a harmonic displacement of the magnet.

Figure 12 shows the WGM shift as a function of the magnet displacement using the data reported in Figure 11. As expected, the sensitivity $d\lambda/dz$ was the same as the one reported in Figure 9 (static measurements). In addition, Figure 11 shows that the hysteresis of the system was negligible in the range of the measured displacement.

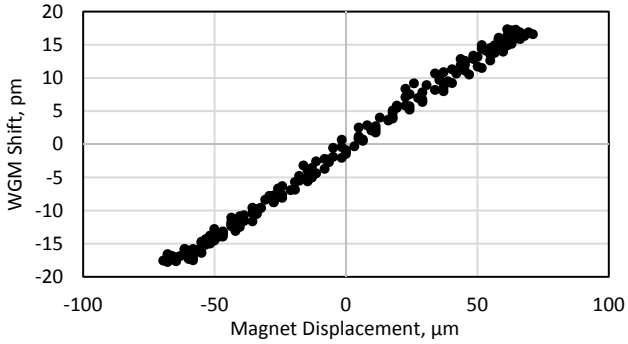

Figure 12. Relationship between the induced WGM shift and the magnet displacement.

Figure 13 shows the sensitivity as a function of the input frequency for four different values of the distance (Z_0) between the sphere and the surface of the permanent magnet.

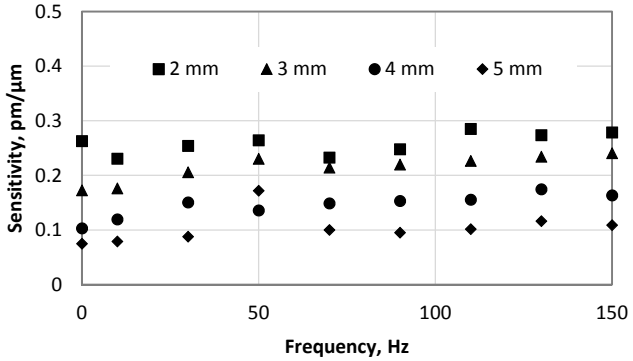

Figure 13. Frequency response of the resonator in the range between 0 and 150 Hz.

As shown in Figure 13, the sensitivity as a function of the input frequency was nearly constant in the investigated frequency range. Again, the sensitivity of the optical resonator decreased with an increase in the distance Z_0 between the microsphere and the surface of the permanent magnet. The maximum frequency range investigated in this study was limited by the hardware used in the

experiments. However, the bandwidth of the proposed sensing technique is limited by the mechanical resonance of the sphere. This limit can be tuned by choosing the sphere's material and size.

In particular, a smaller sphere would lead to a higher bandwidth (smaller sphere's mass), due to the fact that the mechanical resonance occurs later in the frequency spectrum. In addition, a sphere fabricated with a stiffer material (higher spring constant) would lead to a higher bandwidth. These factors are typical for sensors that rely on mechanical deformation. A softer material would reduce the bandwidth but increase the sensitivity. Thus, sensitivity and bandwidth present a tradeoff.

5. Conclusions

The feasibility of a vibrometer based on the shift of the optical modes of a magnetorheological optical resonator was demonstrated analytically and experimentally. For small displacement, the induced WGM shift is nearly a linear function of the amplitude of the displacement. If a tiny permanent magnet is placed on a vibrating structure, the proposed approach can indeed be used to design a photonic vibrometer. The optical resonator showed a sensitivity up to 0.36 pm/μm and a resolution of 278 nm. The study shows that the sensitivity of the resonator can be increased by using a softer polymer, or by adding particles with higher magnetic permeability. Moreover, as showed by the experiments, the sensitivity can be further increased by reducing the initial distance between the surface of the permanent magnet and the optical resonator. Dynamic measurements were also carried out up to a frequency of 150 Hz. In this frequency range, the frequency response of the optical resonator was constant. In addition, the presented vibrometer does not require a reflective surface and/or focusing lens, and it can be operated at low frequencies without a change in sensitivity.

Author Contributions: E.R. and T.I. conceived the experiments; E.R. performed the measurements at Southern Methodist University during his Ph.D.; E.R. and T.I. analyzed the data; E.R. and T.I. wrote the paper.

Funding: This research was funded by the National Science Foundation through grant CBET-1133876.

Acknowledgments: All sources of funding of the study should be disclosed. Please clearly indicate grants that you have received in support of your research work. Clearly state if you received funds for covering the costs to publish in open access.

Conflicts of Interest: The authors declare no conflict of interest.

References

1. Donati, S.; Norgia, M.; Giuliani, G. Self-mixing differential vibrometer based on electronic channel subtraction. *Appl. Opt.* **2006**, *45*, 7264. [CrossRef] [PubMed]
2. Giuliani, G.; Bozzi-Pietra, S.; Donati, S. Self-mixing laser diode vibrometer. *Meas. Sci. Technol.* **2003**, *14*, 24–32. [CrossRef]
3. Stanbridge, A.B.; Ewins, D.J. Measurement of translational and angular vibration using a scanning laser Doppler vibrometer. In Proceedings of the First International Conference on Vibration Measurements by Laser Techniques: Advances and Applications, Ancona, Italy, 3–5 October 1994; Volume 2358, pp. 37–47. [CrossRef]
4. Rothberg, S.J.; Allen, M.S.; Castellini, P.; Di Maio, D.; Dirckx, J.J.J.; Ewins, D.J.; Halkon, B.J.; Muyshondt, P.; Paone, N.; Ryan, T.; et al. An international review of laser Doppler vibrometry: Making light work of vibration measurement. *Opt. Lasers Eng.* **2017**, *99*, 11–22. [CrossRef]
5. Siringoringo, D.M.; Fujino, Y. Experimental study of laser Doppler vibrometer and ambient vibration for vibration-based damage detection. *Eng. Struct.* **2006**, *28*, 1803–1815. [CrossRef]
6. Siringoringo, D.M.; Fujino, Y. Noncontact operational modal analysis of structural members by laser doppler vibrometer. *Comput. Civ. Infrastruct. Eng.* **2009**, *24*, 249–265. [CrossRef]
7. Muramatsu, N.; Sakurai, N.; Wada, N.; Yamamoto, R.; Tanaka, K.; Asakura, T.; Ishikawa-Takano, Y.; Nevins, D.J. Critical comparison of an accelerometer and a laser Doppler vibrometer for measuring fruit firmness. *Horttechnology* **1997**, *7*, 434–438.

8. Muramatsu, N.; Sakurai, N.; Wada, N.; Yamamoto, R.; Tanaka, K.; Asakura, T.; Ishikawa-Takano, Y.; Nevins, D.J. Remote sensing of fruit textural changes with a laser doppler vibrometer. *J. Am. Soc. Hort. Sci.* **1999**, *125*, 120–127.
9. Rembe, C.; Kadner, L.; Giesen, M. Approaching attometer laser vibrometry. *Rev. Sci. Instrum.* **2016**, *87*. [CrossRef] [PubMed]
10. Maekawa, A.; Noda, M.; Shintani, M.; Suzuki, M. Development of noncontact measurement methods using multiple laser displacement sensors for bending and torsional vibration stresses in piping systems. *Int. J. Press. Vessel Pip.* **2016**, *137*, 38–45. [CrossRef]
11. Maekawa, A.; Noda, M.; Shintani, M. Experimental study on a noncontact method using laser displacement sensors to measure vibration stress in piping systems. *Measurements* **2016**, *79*, 101–111. [CrossRef]
12. Maekawa, A.; Takahashi, T.; Tsuji, T.; Noda, M. Experimental validation of non-contacting measurement method using LED-optical displacement sensors for vibration stress of small-bore piping. *Measurement* **2015**, *71*, 1–10. [CrossRef]
13. Lee, J.J.; Shinozuka, M. Real-time displacement measurement of a flexible bridge using digital image processing techniques. *Exp. Mech.* **2006**, *46*, 105–114. [CrossRef]
14. Yasin, M.; Harun, S.W.; Ahmad, H. The performance of a fiber optic displacement sensor. *Laser Phys. Lett.* **2008**, *58*, 55–58. [CrossRef]
15. Binu, S.; Pillai, V.P.M.; Chandrasekaran, N. Fibre optic displacement sensor for the measurement of amplitude and frequency of vibration. *Opt. Laser Technol.* **2007**, *39*, 1537–1543. [CrossRef]
16. Perrone, G.; Vallan, A. A low-cost optical sensor for noncontact vibration measurements. *IEEE Trans. Instrum. Meas.* **2009**, *58*, 1650–1656. [CrossRef]
17. Wu, N.; Yang, L.; Zhang, H.; Wang, X. Optical excitation and detection of a quartz crystal resonator. In Proceedings of the Smart Sensor Phenomena, Technology, Networks, and Systems Integration, San Diego, CA, USA, 8–12 March 2012; Volume 9436.
18. Milewska, D.; Karpienko, K.; Jędrzejewska-Szczerska, M. Application of thin diamond films in low-coherence fiber-optic Fabry Pérot displacement sensor. *Diam. Relat. Mater.* **2016**, *64*, 169–176. [CrossRef]
19. Li, J.; Neumann, H.; Ramalingam, R. Design, fabrication, and testing of fiber Bragg grating sensors for cryogenic long-range displacement measurement. *Cryogenics* **2015**, *68*, 36–43. [CrossRef]
20. Gokhale, V.J.; Gorman, J.J. Optical Knife-Edge Displacement Measurement with Sub-Picometer Resolution for RF-MEMS. *J. Microelectromech. Syst.* **2018**, *27*, 910–920. [CrossRef]
21. Tapalian, H.C.; Laine, J.P.; Lane, P.A. Thermooptical switches using coated microsphere resonators. *IEEE Photonics Technol. Lett.* **2002**, *14*, 1118–1120. [CrossRef]
22. Little, B.E.; Chu, S.T.; Haus, H.A.; Foresi, J.; Laine, J.P. Microring resonator channel dropping filters. *J. Lightw. Technol.* **1997**, *15*, 998–1005. [CrossRef]
23. Ilchenko, V.; Volikov, P.; Velichansky, V.; Treussart, F.; Lefèvre-Seguin, V.; Raimond, J.-M.; Haroche, S. Strain-tunable high-Q optical microsphere resonator. *Opt. Commun.* **1998**, *145*, 86–90. [CrossRef]
24. Monifi, F.; Ozdemir, S.K.; Yang, L. Tunable add-drop filter using an active whispering gallery mode microcavity. *Appl. Phys. Lett.* **2013**, *103*, 181103. [CrossRef]
25. Rubino, E.; Ioppolo, T. Electrostrictive optical resonators for non-contact displacement measurement. *Appl. Opt.* **2017**, *56*, 229–233. [CrossRef] [PubMed]
26. Ioppolo, T. *Whispering Gallery Mode-Based Micro Optical Sensors for Aerospace Applications*; Polytechnic University: New York, NY, USA, 2008.
27. Rubino, E.; Ioppolo, T. Non-contact photonic displacement sensor based on the morphology dependent resonances. In Proceedings of the 55th AIAA Aerospace Sciences Meeting, Grapevine, TX, USA, 9–13 January 2017; pp. 2–6.
28. Rubino, E. *Magnetic Field and Electric Field Effect on Magnetostrictive and Electrostrictive Photonic Resonators*; Southern Methodist University: Dallas, TX, USA, 2016.
29. Ciminelli, C.; Dell'Olio, F.; Campanella, C.; Armenise, M.N. Photonic technologies for angular velocity sensing. *Adv. Opt. Photonics* **2010**, *2*, 370–404. [CrossRef]
30. Matsko, A.B.; Savchenkov, A.; Ilchenko, V.S.; Maleki, L. Optical gyroscope with whispering gallery mode optical cavities. *Opt. Commun.* **2004**, *233*, 107–112. [CrossRef]
31. Quang, N.; Gupta, N.; Ioppolo, T.; Otugen, V. Whispering gallery mode-based micro-optical sensors for structural health monitoring of composite materials. *J. Mater. Sci.* **2009**, 1560–1571. [CrossRef]

32. Rubino, E.; Ioppolo, T. Magnetic field detection using magnetorheological optical resonators. In Proceedings of the SPIE OPTO 2018, San Francisco, CA, USA, 2–7 February 2018. [CrossRef]
33. Guan, G.; Arnold, S.; Otugen, V. Temperature measurements using a microoptical sensor based on whispering gallery modes. *AIAA J.* **2006**, *44*, 2385–2389. [CrossRef]
34. Ioppolo, T.; Manzo, M. Dome-shaped whispering gallery mode laser for remote wall temperature sensing. *Appl. Opt.* **2014**, *53*, 5065–5069. [CrossRef] [PubMed]
35. Frenkel, M.; Avellan, M.; Guo, Z. Whispering-gallery mode composite sensors for on-chip dynamic temperature monitoring. *Meas. Sci. Technol.* **2013**, *24*. [CrossRef]
36. Dong, C.-H.; He, L.; Xiao, Y.-F.; Gaddam, V.R.; Ozdemir, S.K.; Han, Z.-F.; Guo, G.-C.; Yang, L. Fabrication of high-Q polydimethylsiloxane optical microspheres for thermal sensing. *Appl. Phys. Lett.* **2009**, *94*, 231119. [CrossRef]
37. Ioppolo, T.; Das, N.; Ötügen, M.V. Whispering gallery modes of microspheres in the presence of a changing surrounding medium: A new ray-tracing analysis and sensor experiment. *J. Appl. Phys.* **2010**, *107*, 103105. [CrossRef]
38. Vollmer, F.; Braun, D.; Libchaber, A.; Khoshsima, M.; Teraoka, I.; Arnold, S. Protein detection by optical shift of a resonant microcavity. *Appl. Phys. Lett.* **2002**, *80*, 4057–4059. [CrossRef]
39. Arnold, S.; Khoshsima, M.; Teraoka, I.; Holler, S.; Vollmer, F. Shift of whispering-gallery modes in microspheres by protein adsorption. *Opt. Lett.* **2003**, *28*, 272–274. [CrossRef] [PubMed]
40. Armani, A.M.; Vahala, K.J. Heavy water detection using ultra-high-Q microcavities. *Opt. Lett.* **2006**, *31*, 1896–1898. [CrossRef] [PubMed]
41. Chistiakova, M.V.; Armani, A.M. Optical detection of CO and CO_2 temperature dependent desorption from carbon nanotube clusters. *Nanotechnology* **2014**, *25*, 395201. [CrossRef] [PubMed]
42. Cicek, K.; Eryürek, M.; Kiraz, A. Single-slot hybrid microring resonator hydrogen sensor. *J. Opt. Soc. Am. B* **2017**, *34*, 1465. [CrossRef]
43. Ioppolo, T.; Ötügen, M.V. Magnetorheological polydimethylsiloxane micro-optical resonator. *Opt. Lett.* **2010**, *35*, 2037–2039. [CrossRef] [PubMed]
44. Ioppolo, T.; Otugen, V.; Marcis, K. Magnetic field-induced excitation and optical detection of mechanical modes of microspheres. *J. Appl. Phys.* **2010**, *107*, 123115. [CrossRef]
45. Ioppolo, T.; Kozhevnikov, M.; Stepaniuk, V.; Ötügen, M.V.; Sheverev, V. Micro-optical force sensor concept based on whispering gallery mode resonators. *Appl. Opt.* **2008**, *47*, 3009–3014. [CrossRef] [PubMed]